

# Role of upper ocean processes in the seasonal SST evolution over tropical Indian Ocean in climate forecasting system

Jasti S. Chowdary · Anant Parekh · Sayantani Ojha ·  
C. Gnanaseelan

Received: 30 May 2014 / Accepted: 10 January 2015 / Published online: 24 January 2015  
© Springer-Verlag Berlin Heidelberg 2015

**Abstract** In this study role of upper ocean processes in the evolution of sea surface temperature (SST) seasonal variations over the tropical Indian Ocean (TIO) is investigated in climate forecast system version1 (CFSv1) and version2 (CFSv2). Analysis reveals that CFSv2 could capture seasonal evolution of SST, wind speed and mixed layer depth better than CFSv1 with some biases. Discrepancy in reproducing the evolution of seasonal SST in coupled models leads to bias in the spatial and temporal distribution of precipitation. This has motivated to carry out mixed layer heat budget analysis in determining seasonal evolution of TIO SST. Spatial pattern of mixed layer heat budget from observations and models suggest that the processes responsible for SST tendency differ from region to region over the TIO. Further it is found that models underestimated SST tendency compared to the observations. Misrepresentation of advective processes and heat flux (HF) over the TIO is mainly responsible for the distortion of seasonal SST change in the coupled models. Sub-regional heat budget analysis reveals that CFSv1 is unable to reproduce the annual cycle of mixed layer temperature (MLT) tendency over the Arabian Sea, while CFSv2 captured the annual cycle of SST with systematic cold bias. Misrepresentation of the annual cycles of net HF and horizontal advection (Hadv) are accountable for the low rate of change of MLT during most of the year. Hadv during summer season is underestimated by 50 and 25 % respectively in CFSv1 and CFSv2. Further, CFSv1 fails to simulate MLT tendency due to improper evolution of HF annual cycle over the Bay of Bengal. Though annual cycle of HF in CFSv2 is well represented over the Bay of Bengal, its contribution to

MLT change is underestimated compared to observations. Over the southern TIO region, MLT tendency is dominated by HF and Hadv terms in both observations and models. Contribution of HF to the annual cycle of MLT tendency is underestimated in CFSv1 whereas it is overestimated in CFSv2. Contribution of Hadv to MLT change is underestimated by about 50 % in CFSv1 and 10–20 % in CFSv2 over southern TIO. These errors in HF and Hadv are associated with biases in HF components and surface wind representation. Evolution of lead–lag relationship between HF and MLT/SST in both the observations and models suggest the importance of HF in SST evolution over the TIO region. Over all, CFSv2 produced better SST seasonal/annual cycle in spite of having cold bias. This improvement in CFSv2 may be attributed to better cloud–aerosol–radiation physics, which reduces radiation biases. Updated land-surface, ocean and sea ice processes and ocean component may be responsible for improved circulation and annual cycle of ocean–atmospheric components (winds and ocean circulation). However, there is a requirement for improved parameterization of turbulent HF and radiation estimates in CFSv2 to reduce the cold SST bias.

**Keywords** Seasonal cycle · Sea surface temperature · Tropical Indian Ocean · Surface heat flux · Coupled models

## 1 Introduction

Climatically tropical Indian Ocean (TIO) sea surface temperature (SST) is important because of its influence on the Indian summer monsoon (ISM; e.g., Izumo et al. 2008; Annamalai 2010; Boschat et al. 2012), east African monsoon (e.g., Behera et al. 2005) and Australian monsoon (Yoo et al. 2006; Taschetto et al. 2011., references therein).

J. S. Chowdary · A. Parekh (✉) · S. Ojha · C. Gnanaseelan  
Indian Institute of Tropical Meteorology, Pune 411008, India  
e-mail: anant@tropmet.res.in

Eastern Indian Ocean is characterized by zonal winds and warmer SST ( $>28^{\circ}\text{C}$ ), while the western Indian Ocean exhibits meridional circulation and cooler SST. During summer, the cooling by upwelling off Somalia keeps atmospheric convection away from the western Arabian Sea. SST is high and conducive to atmospheric deep convection over the rest of the TIO. The periodic reversals in surface winds drive corresponding reversals in the upper ocean currents and affect the spatial distribution of TIO SST (e.g., Perigaud and Delecluse 1992; McCreary et al. 1993), which plays a key role in determining monsoon rainfall variability (e.g., Clark et al. 2000). Further, part of the largest warm pool on Earth extends from western Pacific to TIO and interacts with the atmosphere. Thus TIO SST plays a significant role in shaping climate on both regional and global scales (Schott et al. 2009).

Even though current coupled general circulation models (CGCMs) simulate a substantially more realistic distribution of ISM rainfall compared to forced atmospheric general circulation models due to the realistic air–sea coupling in the monsoon variability (Wang et al. 2004, 2008, 2009; Krishna Kumar et al. 2005; Wu and Kirtman 2007), a major limiting factor for current CGCMs comes from model deficiencies in capturing SST over the Indian Ocean, especially during boreal summer and fall (Prodhomme et al. 2014). Large systematic biases in the simulated SST over the TIO in many of Intergovernmental Panel on Climate Change-Fourth Assessment Report (IPCC-AR4) coupled models, often exceeding 50 % of the climatological values, are reported by Bollasina and Ming (2013). Prediction skill for the seasonal tropical SST anomalies is closely linked to the models ability in simulating the SST mean state (Lee et al. 2010). SST biases in coupled models drastically limit our understanding of the physical processes involved in the climate fluctuations (e.g., Prodhomme et al. 2014).

TIO exhibits a number of modes of climate variability, ranging from intraseasonal-to-interannual and longer time scales, most of which are coupled to the strong seasonal cycle (Schott et al. 2009). Lee et al. (2010) demonstrated that many coupled models display significant biases in representing the seasonal cycle in Indian Ocean SST and those models have difficulty in capturing the second annual mode in precipitation. Therefore, accurate representation of seasonal SST requires a better understanding of contributions from upper ocean processes. Most of the earlier studies investigated the impact of Indian Ocean SST bias on atmospheric circulation and precipitation (e.g., Prodhomme et al. 2014; Levine et al. 2013; Chaudhari et al. 2013; Chowdary et al. 2014). None of the previous coupled model studies examined the role of upper ocean processes in the evolution of TIO SST seasonal cycle. The present study addresses the mixed layer processes responsible for the seasonal cycle of SST in the TIO in two CGCMs of National Centers

for Environmental Prediction (NCEP) climate forecasting system (CFS) version 1 (CFSv1; Saha et al. 2006) and 2 (CFSv2; Saha et al. 2014). Currently CFS is being used for operational seasonal and extended range ISM forecast/prediction (e.g., Sahai et al. 2013; Saha Subodh et al. 2014).

The paper is organized as follows: in Sect. 2, we briefly describe the details of different data, methodology and models used in the study. Section 3 presents the evolution of seasonal cycle of SST, mixed layer, surface winds and precipitation over the TIO. Spatial pattern of mixed layer processes contributing to the seasonal SST changes are discussed in Sect. 4. Section 5 presents the annual cycle of sub-regional mixed layer heat budget. Section 6 discusses bias in heat flux components and SST and Sect. 7 provides summary.

## 2 Data, methodology and models

The NCEP CFSv1 is a fully coupled ocean–land–atmosphere dynamical seasonal prediction system (Saha et al. 2006) composed of the NCEP Global Forecast System (GFS) atmospheric general circulation model (Moorthi et al. 2001) and the Geophysical Fluid Dynamics Laboratory (GFDL) Modular Ocean Model version 3 (MOM3) (Pacanowski and Griffies 1999). The oceanic component of CFSv1, MOM3 uses spherical coordinates in the horizontal and  $z$  coordinate in the vertical. The zonal resolution is  $1^{\circ}$ , and the meridional resolution is  $1/3^{\circ}$  between  $10^{\circ}\text{S}$  and  $10^{\circ}\text{N}$  and gradually decreases pole ward. Recently NCEP developed CFSv2, which is a fully coupled ocean–atmosphere–land model with advanced physics, increased resolution and refined initialization (Saha et al. 2014). CFSv2 consists of a spectral atmospheric model at a resolution of T126 ( $\sim 0.937^{\circ}$ ) with 64 hybrid vertical levels and the (GFDL MOM4p0) ocean model (Griffies et al. 2004) at  $0.25^{\circ}$ – $0.5^{\circ}$  grid spacing with 40 vertical layers. The atmosphere and ocean models are coupled with no flux adjustment. It uses rapid radiative transfer model shortwave radiation with maximum random cloud overlap (Iacono et al. 2000; Clough et al. 2005). It is also coupled to a four-layer Noah land surface model (Ek et al. 2003) and a two-layer sea ice model (Wu et al. 2005). Compared to CFSv1, the CFSv2 incorporates improved physics for cloud–aerosol–radiation, land surface, ocean and sea ice processes, in addition to a new atmosphere–ocean–land data assimilation system (Saha et al. 2014). CFSv1 (CFSv2) free run data from last 20 years out of 100 (30) years is considered for the analysis as in Saha Subodh et al. (2014) and Pokhrel et al. (2012). Both the versions of CFS model have been ported on IBM Prithvi High Performance Computing system at Indian Institute of Tropical Meteorology, Pune, India.

Long term mean ocean temperature data from World Ocean Atlas 2009 (WOA 09) (Locarnini et al. 2010) and

precipitation from Center for Climate Prediction merged analysis (CMAP; Xie and Arkin 1996) products are used for comparison. Ocean surface flux components are compared with the state of the art TropFlux air-sea flux product (Praveen Kumar et al. 2010). Further, upper ocean advective processes in CFSv1 and CFSv2 are compared with the Simple Ocean Data Assimilation (SODA version 2.1.6) reanalysis (Carton and Giese 2008). SODA assimilates temperature and salinity profiles from the World Ocean Atlas (MBT, XBT, CTD, and station data), as well as additional hydrography, SST, and altimeter sea level. The ocean model is based on Parallel Ocean Program physics with an average  $0.25^\circ \times 0.4^\circ \times 40$ -level resolution. SODA analysis generally provides more accurate estimates of mean heat advection than models with no data assimilation. Zheng et al. (2011) reported that SODA surface currents are reasonably good when compared to near-real-time ocean surface currents derived from satellite data of Ocean Surface Current Analyses Real Time products. Mixed layer temperature (MLT) or SST tendency equation used in the present study to estimate different upper ocean heat budget terms is

$$\frac{\partial T_m}{\partial t} = \frac{Q_0 - Q_p}{\rho C_p H_m} - \frac{w_e(T_m - T_b)}{H_m} - U \cdot \nabla T_m - K_z \frac{\partial^2 T_m}{\partial z^2} + Res \tag{1}$$

where  $T_m$  denotes mixed layer temperature.  $\partial T_m / \partial t$  is the rate of change of  $T_m$ ,  $\rho$  is seawater density ( $1,025 \text{ kg m}^{-3}$ ),  $C_p$  is heat capacity of Sea water ( $4,186 \text{ J kg}^{-1} \text{ K}^{-1}$ ),  $H_m$  is mixed layer depth (MLD),  $Q_0$  is the net surface heat flux ( $\text{W/m}^2$ ),  $Q_p$  is the shortwave radiation ( $\text{W/m}^2$ ) penetrating below the mixed layer,  $w_e$  is the entrainment rate (m/s), and  $T_b$  is the temperature at the bottom of mixed layer (e.g., Qiu 2000; Qu 2003; Du et al. 2005).  $K_z$  is the coefficient of vertical diffusion of heat ( $0.1 \times 10^{-4} \text{ m}^2 \text{ s}^{-1}$ ).  $Res$  is residual term.  $Q_p$  is calculated based on Pacanowski and Griffies (1999) empirical formula given below

$$Q_p = Q_s \left[ R_1 e^{-\frac{H_m}{\gamma_1}} + R_2 e^{-\frac{H_m}{\gamma_2}} \right] \tag{2}$$

where  $Q_s$  is the net surface shortwave radiation,  $R_1$  and  $R_2$  are separation constants equal to 0.58 and 0.42 respectively.  $\gamma_1$  and  $\gamma_2$  are the attenuation lengths equal to 0.35 and 23 m, respectively.

The entrainment rate  $w_e$  is determined based on Qu (2003) as follows

$$w_e = \frac{\partial H_m}{\partial t} + w_b + U \cdot \nabla H_m \quad \text{if } \frac{\partial H_m}{\partial t} + w_b + U \cdot \nabla H_m > 0 \quad \text{else } w_e = 0 \tag{3}$$

where  $\partial H_m / \partial t$  denotes the rate of change of mixed layer depth,  $w_b$  is the vertical velocity of water parcel at the base

of the mixed layer, and  $U \cdot \nabla H_m$  is the divergence of horizontal advection of water at bottom of the mixed layer.

Horizontal advection term in the Eq. (1) is

$$U \cdot \nabla T_m = u \frac{\partial T_m}{\partial x} + v \frac{\partial T_m}{\partial y} \tag{4}$$

where  $u$  is zonal and  $v$  is meridional currents averaged within the mixed layer. Observed ocean data is interpolated to model vertical levels. As model upper most layer is 5 m depth we have considered temperature drop of  $0.8^\circ \text{C}$  for MLD calculation (e.g., Kara et al. 2003). Left hand side term of Eq. (1) is referred to as the temperature tendency, first term in right hand side is referred as heat flux (HF), second is entrainment ( $w_e$ ), third is horizontal advection (Hadv) and fourth term is vertical diffusion (Vdif), respectively. Seasons refer to that of northern hemisphere.

### 3 Evolution of seasonal cycle over the TIO

#### 3.1 Seasonal mean SST, MLD and surface winds

Spatial distribution of seasonal SST, MLD and surface winds is illustrated in Fig. 1 for observations, CFSv1 and CFSv2. Warm SST above  $29^\circ \text{C}$  during spring is apparent in the region north of  $5^\circ \text{S}$  in observations and CFSv1 (Fig. 1a, e). In case of CFSv2 SST is lower than observations by about  $1^\circ \text{C}$  throughout the basin (Fig. 1i). MLD is deeper in both models as compared to observations over most of TIO region. Weak westerly winds over the equatorial Indian Ocean (EIO) region (Fig. 1a) are important in driving ocean currents there. These winds are weak in CFSv2 and are replaced by weak easterlies in CFSv1. Misrepresentation of surface wind may strongly influence the ocean dynamics. By summer strong southerly winds over the northern Indian Ocean (NIO; equator to  $25^\circ \text{N}$  and  $55^\circ \text{E}$  to  $100^\circ \text{E}$ ) region causes for changes in upper ocean properties (Fig. 1b). For example anomalous upwelling associated with these winds cools SST near Sumatra coast. MLD is deep over the central Arabian Sea, which is associated with downwelling. MLD is also deeper in most of the TIO region during summer as compared to spring. These seasonal changes in SST, MLD and winds are well represented in CFSv2 as compared to CFSv1 (Fig. 1f, j). SST is slightly higher over most of the TIO during fall season compared to summer (Fig. 1b, c). Observations show that deep MLD is located south of  $10^\circ \text{S}$  and parts of Arabian Sea in fall. Surface winds are northeasterlies over NIO and westerlies in the equatorial region (Fig. 1c). Though observed seasonal changes of MLD are captured by both models, deep MLD is reported in most of the TIO during fall (Fig. 1g, k). Strong equatorial easterly winds instead of westerly winds are noted in CFSv1, resultant strong zonal gradient in SST

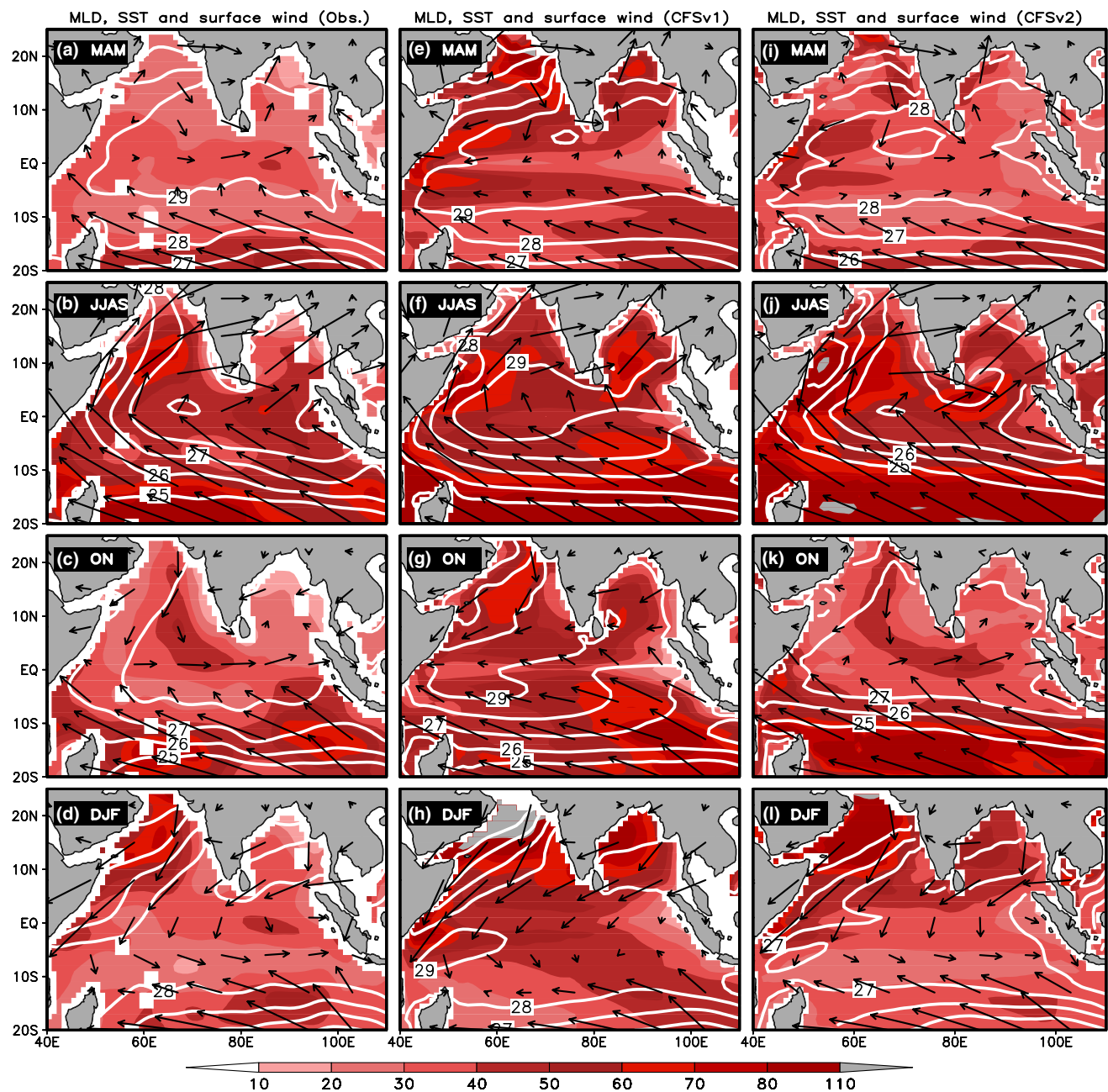


**Fig. 1** Mean seasonal mixed layer depth (m), SST (contours °C) and surface winds (vectors; m/s) from observations for **a** MAM, **b** JJAS, **c** ON and **d** DJF. **e–h** is similar to **a–d** but for CFSv1 and **i–l** is similar to **a–d** but for CFSv2

is reported (Fig. 1g). SST and surface winds are well represented in CFSv2 with weaker magnitude than observations in the east of 60°E over the EIO. By winter, deep MLD, cold SSTs and northeasterly winds are apparent in observations over the NIO (Fig. 1d). These features are fairly well captured by both the models (Fig. 1h, l). However deeper than observed MLD in CFSv1 and CFSv2 are seen throughout the year. While seasonal cycle of SST is well captured in CFSv2, SST is  $\sim 1$  °C lower than the observations in the TIO region. Over all, models are able to capture

the seasonal changes in MLD, SST and surface winds with some discrepancy.

### 3.2 SST tendency and precipitation

The longitude-time evolution of SST and precipitation seasonal cycle (annual mean is removed) averaged from 5°N to 20°N is displayed in Fig. 2a–c for observations, CFSv1 and CFSv2. Observations show warm SST anomalies (with respect to annual means) that begin from March and persist

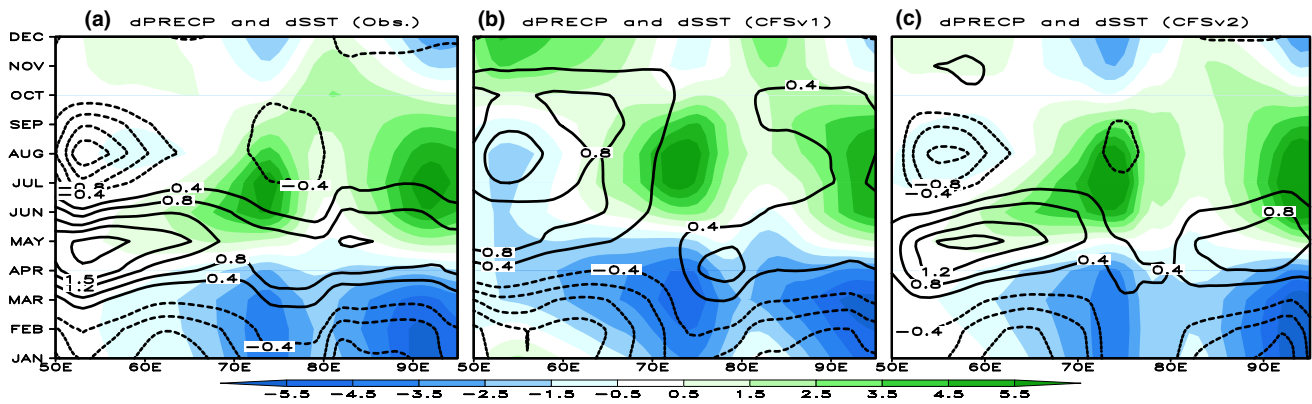


**Fig. 2** Longitude–time plot of precipitation (*shaded*; mm/day) and SST (contours; °C) seasonal cycle (annual mean is removed) over the north Indian Ocean (averaged from 5°N to 20°N) for **a** observations, **b** CFSv1 and **c** CFSv2

until June over the NIO. This warming is conducive for atmospheric deep convection, and positive precipitation anomalies (Fig. 1a). During summer anomalous cold SST anomalies are apparent over the western Arabian Sea with suppressed rainfall there. Over rest of the NIO positive rainfall anomalies are maintained until fall due to warm SST anomalies (with respect to annual mean). During winter cold SST and low rainfall anomalies are consistent with each other. This shows that the seasonal cycle of SST and precipitation anomalies are in coherence with each other (Fig. 2a). Seasonal cycle of precipitation and SST in CFSv1 is not well represented as compared to the observations mainly during spring and summer. Moreover, negative precipitation anomalies during winter persist up to spring season over the NIO region. SST displays positive anomalies (with respect to annual mean) during summer season in CFSv1 unlike in observations. CFSv2 also displayed some discrepancies with low SST between 70 and 80°E and high precipitation over the Bay of Bengal. Therefore, proper evolution of SST seasonal cycle over the Indian Ocean is essential for accurate rainfall evolution. For example, negative SST anomalies over the Arabian Sea extended to April in CFSv1 unlike in observations and CFSv2 (Fig. 2). Consequently, positive precipitation anomaly in CFSv1 is delayed by a month over the ISM region due to error or bias in the SST annual cycle.

Figure 3 shows the spatial distribution of seasonal changes in SST superimposed on precipitation change (tendency) over the TIO region. Seasonal change or tendency in SST (precipitation) for MAM is displayed as MAM minus DJF SST (precipitation) and likewise for JJAS, ON and DJF. Observations show that from winter to spring, precipitation tendency is positive over most of the NIO region with maximum rainfall zone over the head Bay of Bengal and contiguous land regions (Fig. 3a). SST tendency is positive in the entire TIO during spring. SST and rainfall

changes are in coherence with each other over the NIO as shown in Fig. 2. CFSv1 failed to represent such changes in rainfall and to some extent the SST tendency. Rainfall and SST tendency coherence is better represented in CFSv2 as compared to CFSv1 (Fig. 3e, i). Over the southern TIO (STIO; 5°S–20°S and 45°E–100°E) region, SST and rainfall changes are out of phase in models and observations. Changes in rainfall pattern from DJF to MAM are unrealistic (realistic) in CFSv1 (CFSv2).

By summer, observations show that strong positive tendency in rainfall over the entire NIO (monsoon region) and Equatorial Indian Ocean (EIO) regions, whereas rainfall weakens over the western Arabian Sea and STIO regions (Fig. 3b). Increased rainfall tendency over the head Bay of Bengal and eastern Arabian Sea are consistent with the increase in SST tendency from MAM to JJAS. Due to strong upwelling, SST is cooler over the western Arabian Sea where the seasonal rainfall change is negative. Similarly, negative SST tendency in the STIO due to strong south-easterlies and negative rainfall tendency are apparent in observations. Both CFSv1 and CFSv2 have represented the changes in SST and precipitation tendency pattern over the STIO well with some differences in magnitude (Fig. 3f, j). However, SST changes in CFSv1 display discrepancies over the NIO and western EIO (WEIO; 10°S–10°N and 50°E–70°E) regions and associated rainfall also shows unrealistic changes (positive) there. Rate of cooling in SST from spring to summer over the EIO region is higher in CFSv2 by 0.5 °C than in observations. On the other hand, rainfall change over this region is low in the model compared to observations. This shows that CFSv2 also has discrepancy in representing changes in SST and precipitation. In CFSv2 strong rate of change of SST over the STIO is coherent with strong negative precipitation tendency (Fig. 3j). Negative SST bias in models over the eastern Bay of Bengal, with respect to

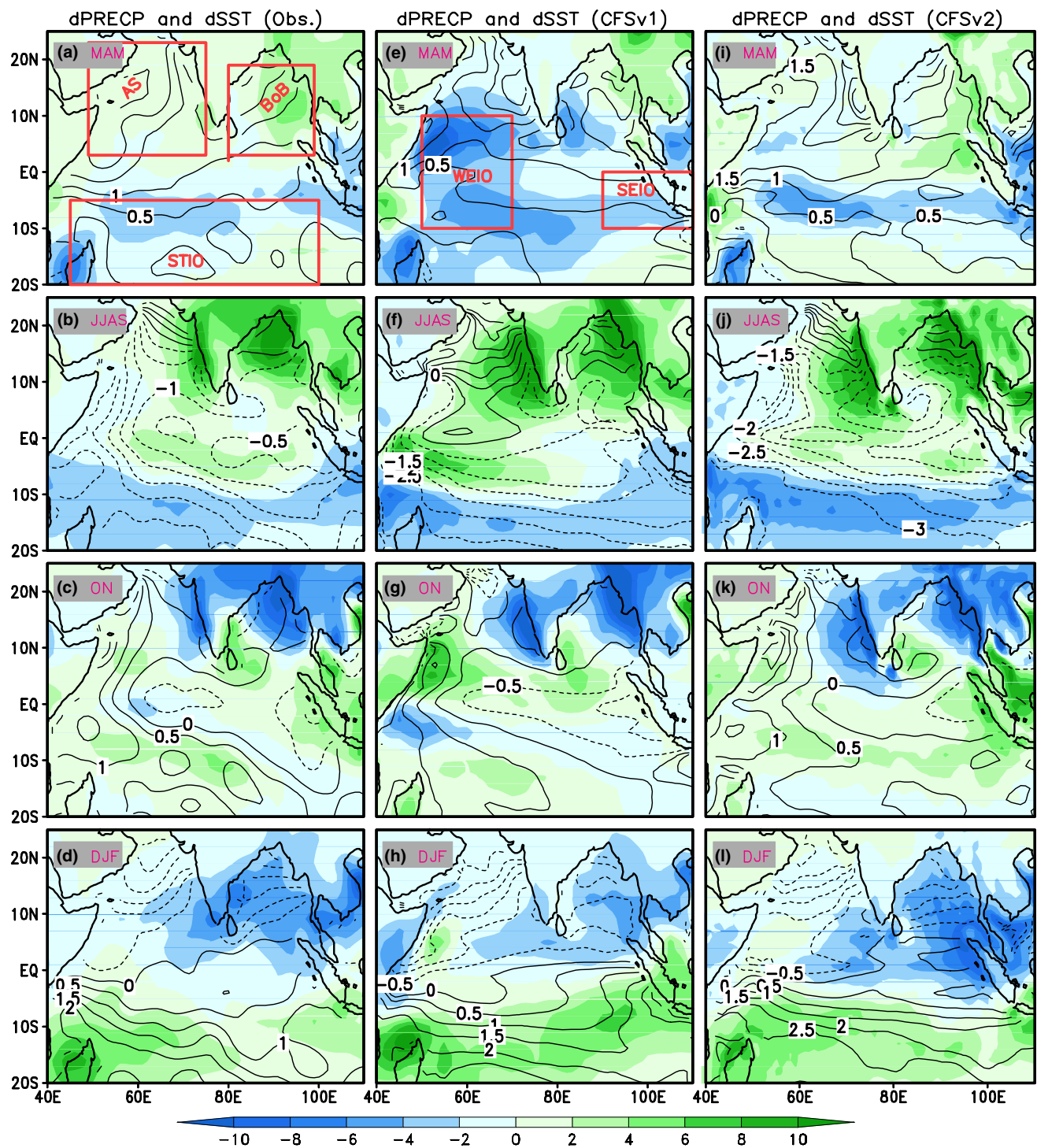


**Fig. 3** Seasonal tendency of precipitation (dPRECP; mm/day) and SST (dSST; contours °C) from observations for **a** MAM minus DJF, **b** JJAS minus MAM, **c** ON minus JJAS and **d** DJF minus ON. **e–h** is

similar to **a–d** but for CFSv1 and **i–l** is similar to **a–d** but for CFSv2. Sub-regions of TIO that are used for area averaged heat budget analysis are represented with rectangular boxes in **a** and **e**

observations, is mainly responsible for dry bias over the east coast of India.

During fall, rainfall decreases drastically over the ISM region as compared to summer and increases over the

maritime continent and south of the equator (Fig. 3c). SSTs are warmer over the western TIO and STIO in fall than summer. In contrast CFSv1 shows strong positive rainfall tendency over the western Arabian Sea and negative SST

over the EIO region (Fig. 3g). Unrealistic negative precipitation tendency is also seen in south of equator over western TIO. Though seasonal changes in SST and precipitation are well represented in CFSv2 compared to CFSv1, negative (positive) SST (precipitation) anomalies over the EIO (southeast TIO) region is underestimated (overestimated) compared to observations (Fig. 3c, k). By winter, observations show that SST and rainfall changes are asymmetric to the equator with negative sign in the north and positive in the south of equator (Fig. 3d). Magnitude of rainfall tendency over the NIO is less in CFSv1 compared to the observations (Fig. 3h). Negative rainfall tendency band extended to EIO region in CFSv2 unlike in observations (Fig. 3l). The amplitude of SST change in CFSv2 is higher than in CFSv1 over the SIO region. Overall, SST seasonal change appears to have strong influence on precipitation seasonal cycles in different regions of TIO.

Therefore the representation of seasonal SST and its tendency over the TIO are very important for any dynamical operational forecasting system. Any discrepancy in reproducing the seasonal evolution of SST would lead to biases in precipitation. This has motivated us to examine the contribution of different mixed layer terms in determining the seasonal SST changes (SST tendency) over the TIO in the forecast models CFSv1 and CFSv2. In the next section we have examined the spatial pattern of mixed layer processes which are responsible for seasonal changes in SST by calculating each term of the Eq. 1 before proceeding to regional heat budget analysis. For example, SST tendency (MAM SST minus DJF SST) and heat budget terms (right hand side of Eq. 1) during spring are analyzed concurrently. Figure 3a, b show the regions (rectangular boxes) selected for area averaged heat budget analysis.

#### 4 Contribution of mixed layer processes to seasonal SST changes over the TIO: spatial patterns

##### 4.1 Spring

Contribution of spring net heat flux term (HF) to SST tendency is shown in Fig. 4a for observations. HF contributes positively to SST changes from DJF to MAM in most of the TIO (north of 17°S). Spatial pattern of strong HF contribution to SST change is extended from western EIO to east in CFSv1, which is unrealistic compared to observations (Fig. 4b). Contribution of HF to SST change is much stronger (negative) in CFSv2 compared to the observations in the region south of 17°S, corresponding negative change in SST is noted in the east of Madagascar unlike in observations (Fig. 4a, c). Further, strong positive contribution from HF over the eastern EIO in the model is noted and which is not seen in the observations. This infers the

importance of representing the spatial distribution of heat flux for proper SST seasonal changes in coupled models.

The seasonal cycle of SST is also influenced by the ocean circulation through oceanic advection (e.g., Hogg et al. 2008). Maximum contribution of entrainment velocity ( $w_e$ ) to SST cooling from DJF to MAM is located over southwest TIO in observations and in CFSv2 (Fig. 4d, f). Note that the contribution of upward vertical velocity is only considered, as the downward velocity may not have any impact on SST. In case of CFSv1, major contribution of  $w_e$  is confined over the equatorial region (Fig. 4e). This misrepresentation in CFSv1 is due to the bias in vertical entrainment and is consistent with easterly wind bias. Contribution of  $w_e$  to SST change is also evident over WEIO in the observations and models. At the same time, SST tendency is positive throughout the basin. This indicates that DJF to MAM HF plays a vital role in controlling SSTs (Fig. 4a–c). However, regions in which  $w_e$  is contributing opposite to heat flux are affected by change in the SST magnitude. This indicates that spatial distribution of  $w_e$  would influence the SST change from DJF to MAM. Therefore, proper representation of  $w_e$  in coupled models is also important.

Contribution of horizontal advection of temperature (Hadv) in SST change is shown in Fig. 4d–f. Hadv is positively contributing to SST seasonal change from DJF to MAM over extreme southeast TIO, which is apparent in CFSv2 as well. However, the magnitude of Hadv is weak in CFSv1 as compared to CFSv2 (Fig. 4e). This shows that CFSv1 has problems in representing advection properly during spring, which is mainly due to improper changes in seasonal winds (Fig. 1). This analysis shows that SST change from DJF to MAM is highly controlled by HF in the region north of 5°S, while Hadv contributed positively to SST change in south of 5°S. These features are well represented in CFSv2 as compared to the CFSv1.

##### 4.2 Summer

The SST tendency (from MAM to JJAS) south of 15°N during summer displays cooling (maximum exceeding 3 °C over the western Arabian Sea) in the observations and CFSv2 (Fig. 4g, i). In contrast CFSv1 displays a positive SST tendency over most of the Arabian Sea. This is due to the strong positive contribution from HF in the model compared to the observations (Fig. 4h, g). It is important to note that HF contribution to SST is favorable for warming over the central Arabian Sea in both the observations and CFSv2, but SST cools (Fig. 3i), which strongly indicates the role of ocean dynamics in determining the SST tendency. Both HF and SST tendency are in phase with stronger cooling from MAM to JJAS over STIO in the observations and the models. This indicates that seasonal

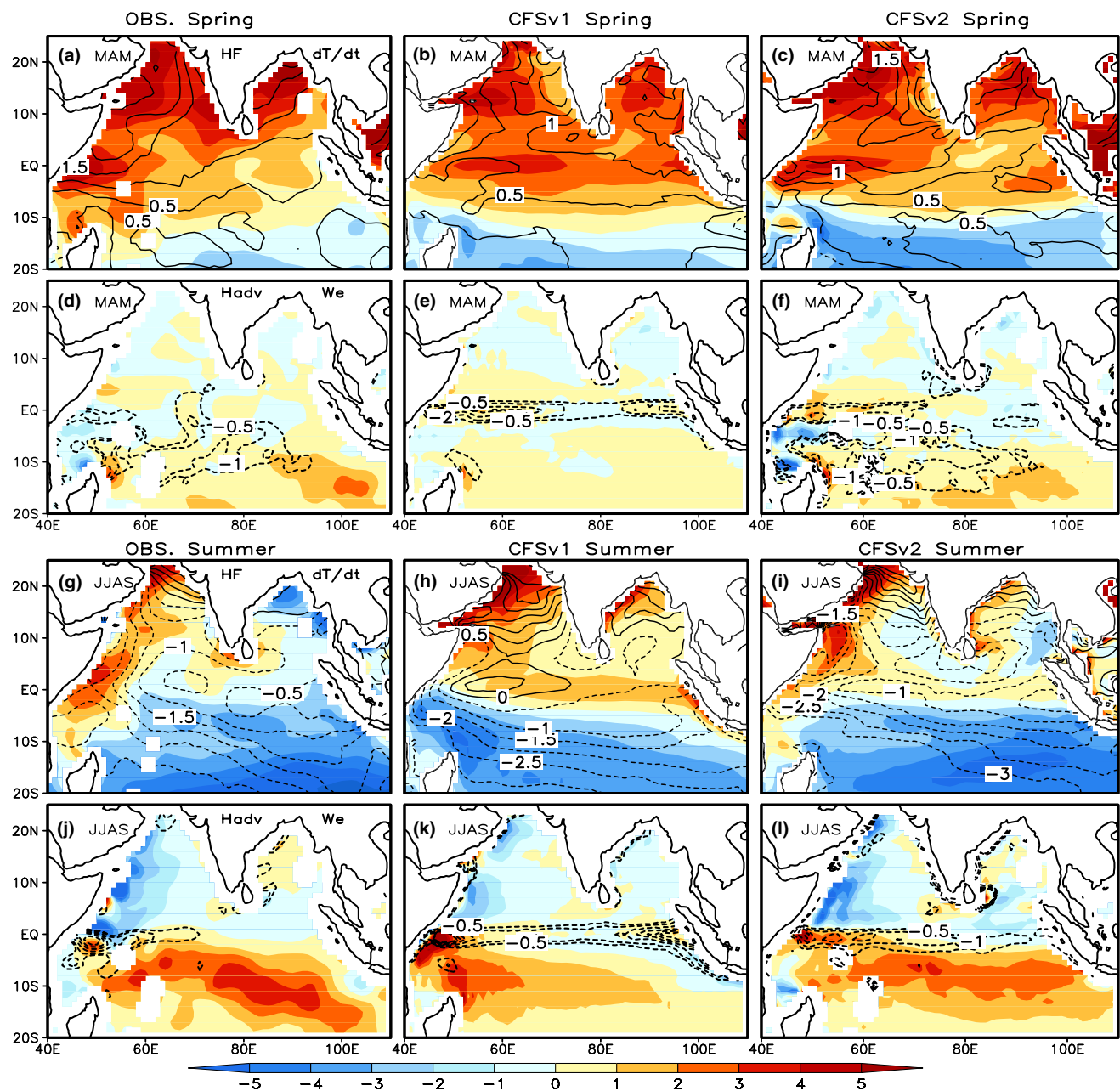


**Fig. 4** **a** Contribution of heat flux term (HF; shaded, positive is warming;  $^{\circ}\text{C}$ ) and SST seasonal tendency (contours  $^{\circ}\text{C}$ ) and **d** contribution of horizontal advection (Hadv; shaded,  $^{\circ}\text{C}$ ) and entrainment (ent (We); contours,  $^{\circ}\text{C}$ ) to SST tendency for observations during

Spring (MAM) season. **b** and **e** is similar to **a** and **d** but for CFSv1 and **c** and **f** is similar to **a** and **d** but for CFSv2, **g–i** is similar to **a–f** but for summer (JJAS) season

SST over STIO region is strongly influenced by heat flux variations. Rate of change in SST from spring to summer is higher ( $\sim 4^{\circ}\text{C}$ ) in CFSv2 compared to the observation ( $\sim 3^{\circ}\text{C}$ ) over STIO region. This is due to the excess loss of net heat flux in CFSv2.

Vertical entrainment contributes negatively to SST change from MAM to JJAS over WEIO in the observations (Fig. 4j, l). The negative  $w_e$  is in-phase with SST tendency over the EIO and in some parts of NIO, such as Somalia

coast. CFSv1 displayed unrealistic upward vertical velocities over the eastern EIO region and contributed for excess cooling by more than  $0.5^{\circ}\text{C}$  as compared to the observations (Fig. 4h, k). In CFSv2  $w_e$  contributed (negatively) strongly to SST change in east of Sri Lanka by as much as  $0.5^{\circ}\text{C}$  greater than the observed cooling (Fig. 4i, l). This unrealistic  $w_e$  is mainly due to improper surface wind representation in models (Fig. 1). Further, vertical entrainment in the coupled models has contributed less cooling



over western Arabian Sea than in the observations. This is mainly due to weak upwelling associated with the weak southwest monsoon flow in the models (Fig. 1). However, the spatial pattern of  $w_e$  is better represented in CFSv2 than in CFSv1 (Fig. 4k, l). It is important to note that low resolution models may be contributing for errors in the advective processes near coastal regions.

During summer horizontal advection contributes to SST cooling over the western and central Arabian Sea by advecting cold upwelled water from Somali Coast (e.g., Shankar et al. 2002; de Boyer Montegut et al. 2007; Fig. 4j–l). These advective processes are well represented in both the models but the magnitude is underestimated (about 1–2 °C; Fig. 4k, l). The role of Hadv in controlling the SST changes from spring to summer in the western Arabian Sea is dominant compared to HF. The cooling induced by Hadv from MAM to JJAS over this region is as much as 4, 2 and 3 °C in the observations, CFSv1 and CFSv2 respectively. In the STIO, Hadv contributes positively to SST tendency for observation and models; however the HF is the dominant contributor to the SST change there. Though CFSv1 shows some contribution (negatively) from vertical and horizontal advection to SST change over the western Arabian Sea, strong heat flux controlled SST unlike in CFSv2 and the observations. In short errors in the seasonality of upper ocean processes would lead to biases in SST seasonal cycle in CFSv1.

#### 4.3 Fall

As the southwesterly monsoon winds are relaxed by boreal fall season in most of the TIO (Fig. 1), SST warms due to reduced evaporation and enhanced shortwave radiation (SWR) relative to JJAS in observation and in the models. However, SST tendency is negative over the central and eastern EIO (Fig. 5a). This SST change is out of phase with HF over the EIO (Fig. 5a–c), suggesting that the oceanic processes are important for SST change in this region. Out of phase relationship between SST tendency and HF is also seen over the northern Bay of Bengal in both the models, especially in CFSv2. HF contribution to the SST tendency over the NIO is weaker in CFSv1 compare to CFSv2 and observations. The maximum contribution of HF in SST change is evident over the western TIO in the observations and models, indicating strong SST–flux relationship. During fall  $w_e$  is strong over WEIO and negatively contributing to SST changes in observations and CFSv2 (Fig. 5d, f), which is not the case for CFSv1 (Fig. 5e). SST tendency shows warming from JJAS to ON over the western Arabian Sea but  $w_e$  contributes negatively in both models. This further indicates the impact of heat flux in controlling the SST seasonal change. The  $w_e$  is negative over eastern EIO in CFSv1 and is much stronger than observations and CFSv2

(Fig. 5d–f). Impact of  $w_e$  on SST change is apparent in CFSv1 over eastern EIO unlike in observations and CFSv2. This indicates large errors in the spatial distribution of  $w_e$  in CFSv1.

During ON, both HF and Hadv are contributing positively to warm SST over the SIO, whereas  $w_e$  contributes negatively (Fig. 5d). These features are clear in both the observations and models but the magnitude of Hadv is underestimated in CFSv1 by about 50 % over this region (Fig. 5e). Moreover, the magnitude of Hadv is underestimated over the WEIO by both models. Over the southeastern TIO, Hadv contributed (strong) positively to SST changes whereas HF contributed negatively. Thus the SST warming over this region is balanced by both HF and Hadv. These features are well represented in CFSv2 as compared to CFSv1 (Fig. 5e, f).

#### 4.4 Winter

SST tendency shows negative sign in the region north of the equator and positive in the south from fall to winter. SST drop from ON to DJF over the NIO is highly influenced by HF (Fig. 5g–i). Similarly, HF contribution in controlling SST in DJF over STIO is strong. The warming induced by HF is highest over the southwest TIO and is well represented by CFSv2 (Fig. 5i). In case of CFSv1, contribution of HF is maximum over the eastern EIO and southwest TIO. Both models underestimated the heat flux loss over Bay of Bengal. However, over the Arabian Sea models do capture the heat flux loss and are consistent with observed SST tendency.

During winter strong entrainment is noted over the WEIO and STIO regions (Fig. 5j). CFSv1 underestimates the magnitude of  $w_e$  over the equatorial region than in the observations (Fig. 5j, k). Over STIO region both models underestimated the contribution of vertical velocities to SST change. CFSv2 displayed better spatial pattern of  $w_e$  contribution to SST than in CFSv1. It is important to note that the SST tendency is mostly dominated by HF over NIO and STIO. From ON to DJF, Hadv is contributed positively in the regions away from the equator and negatively near the equator (Fig. 5j–l). But SST tendency is negative north of the equator and positive in the south. This shows that Hadv contributes towards SST change (tendency) in STIO to some extent but not in NIO. The contribution of Hadv in winter is weak compared to that of summer and fall, and is evident in both the observations and models. During DJF strong Hadv is evident off Somalia in CFSv1, contributing positively to SST tendency. It is clear from Figs. 4 and 5 that CFSv2 represents the spatial distribution of horizontal advection better compared to CFSv1 in all seasons.

This section summarizes that seasonal SST tendency over the Arabian Sea and Bay of Bengal is controlled by

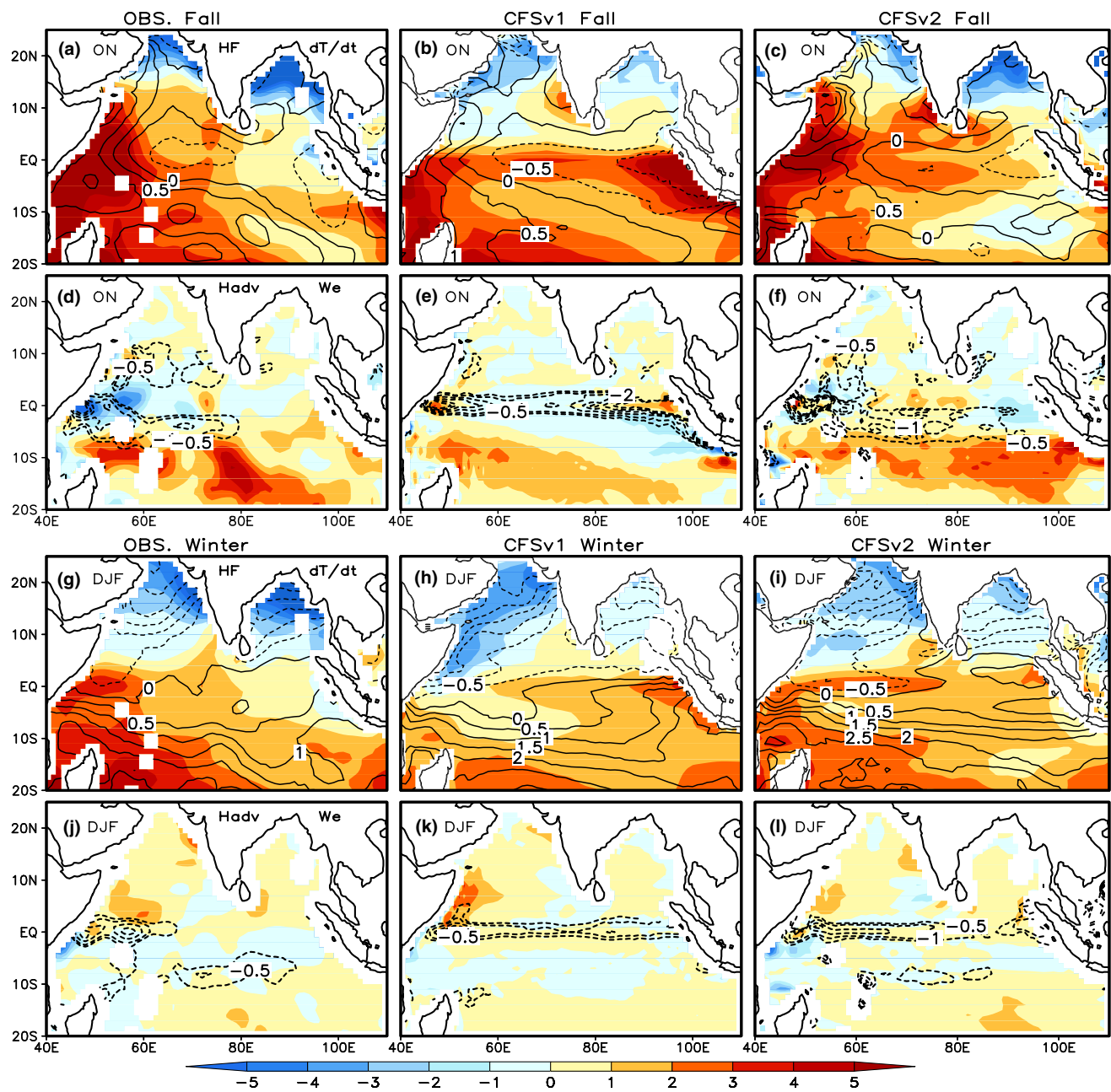


**Fig. 5** Same as Fig. 4 but for fall (ON) and winter (DJF) seasons

heat flux from winter to spring, while from spring to summer, SST tendency is highly controlled by horizontal advection. SST tendency from summer to fall and fall to winter is affected by heat flux. Over the EIO region SST tendency from winter to spring and fall to winter are completely dominated by heat flux. SST tendency in some parts of EIO from spring to summer and summer to fall is controlled by vertical and horizontal advection. Over the STIO both heat flux and Hadv contribute to SST tendency from winter to spring. During summer (winter), SST cooling (warming) in STIO is highly controlled by negative

(positive) heat flux. While warming from summer to fall is determined by both heat flux and horizontal advection. It is noted that during spring (from DJF) NIO (area average) warmed (SST tendency) by  $1.6^{\circ}\text{C}$  in the observations whereas it is  $1.25^{\circ}\text{C}$  ( $1.06^{\circ}\text{C}$ ) in CFSv2 (CFSv1). During summer over the western Arabian Sea observed change in SST is  $-2.0^{\circ}\text{C}$ , whereas in CFSv2 (CFSv1) change is  $-2.21^{\circ}\text{C}$  ( $-0.41^{\circ}\text{C}$ ). In fall observed SST tendency is  $0.5^{\circ}\text{C}$  over the STIO and is  $1.40^{\circ}\text{C}$  ( $2.38^{\circ}\text{C}$ ) in CFSv2 (CFSv1). During winter over the NIO SST tendency is  $-1.96^{\circ}\text{C}$  in observations, while in CFSv2 (CFSv1) it is

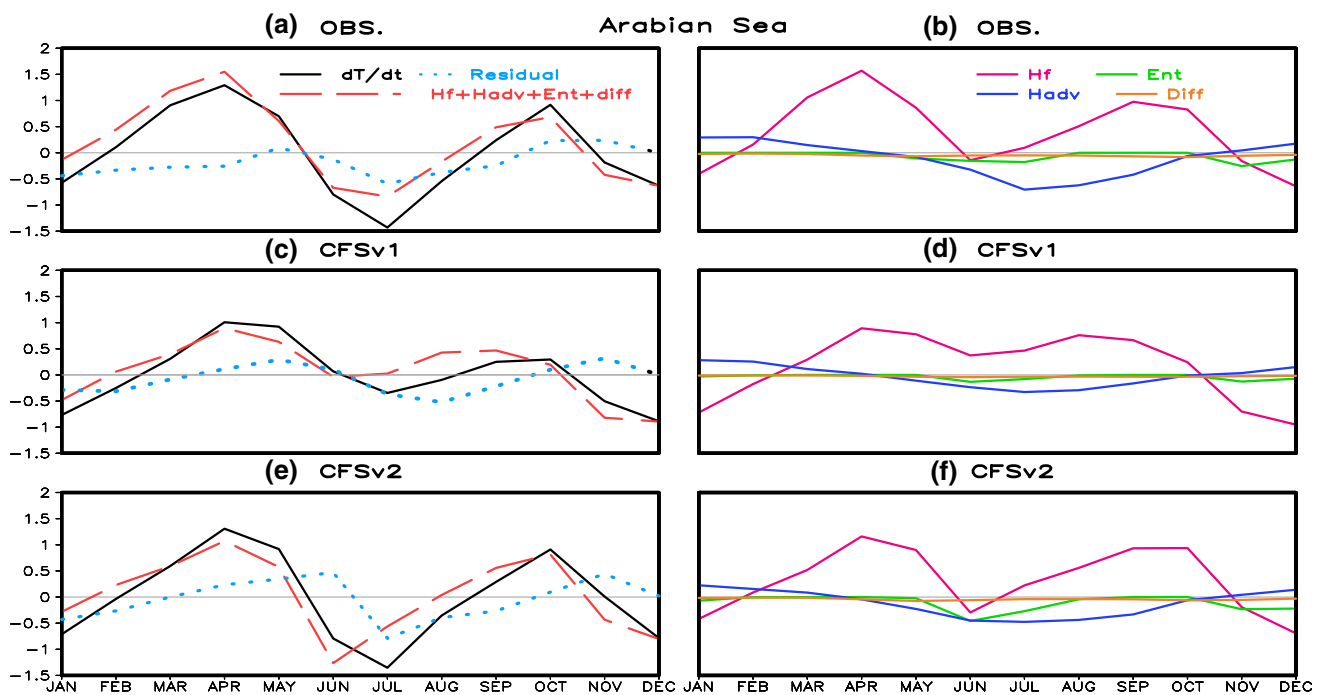


**Fig. 6** Observed annual cycle of the Arabian Sea **a** sum of HF and advective processes, MLT tendency and residual **b** contribution of individual processes/terms to MLT tendency, **c** and **d** are same as **a**

and **b** but for CFSv1 and **e** and **f** are same as **a** and **b** but for CFSv2. Units are in °C/month

−1.4 °C (−2.4 °C). Further seasonal SST tendency over STIO is highly influenced by heat flux in CFSv2 unlike in observations. Likewise, SST seasonal tendency in the NIO is not well represented due to heat flux and advection problems in CFSv1. Most importantly seasonal cycle of SST over the EIO region is not well represented in CFSv1 due to improper advective processes (Figs. 4, 5).

Generally, CFSv1 overestimated contribution of  $w_e$  to seasonal SST over the EIO region and underestimated over the off equatorial regions, especially over the western Arabian Sea and southwest TIO. This misrepresentation of  $w_e$  is well reflected in the spatial pattern of SST tendency. CFSv2 also overestimated  $w_e$  over the east coast of India and southern tip of India, which in fact shows certain influence on SST seasonal cycle. Though the contribution of  $w_e$  to seasonal change in TIO SST is limited to some particular regions, it is important to represent  $w_e$  well in the models. This analysis clearly shows that in models the contribution of HF to seasonal SST is overestimated in some regions and underestimated in some other regions of TIO. For example over the STIO, HF contribution to SST change in MAM and JJAS is high in CFSv2 than in CFSv1 (Fig. 4). Spatial distribution of HF is not well organized in CFSv1 which might be responsible for the improper seasonal changes in SST over most of TIO. Further, large biases in heat flux components away from equator are partly responsible for bias in SST.

Overall, magnitude of cooling/warming in various regions of TIO due to different processes is better represented by CFSv2 than in CFSv1. From this section it is clear that seasonal SST/MLT tendency and mixed layer processes are different in various regions of TIO both in the observations and models. To further investigate the role of mixed layer processes on SST at the sub-regional viewpoint, we examined the annual cycle of different components over the Arabian Sea, Bay of Bengal, WEIO, Southeast EIO (SEIO; Equator to 10°S and 90°E–110°E) and STIO in both models and observations. In addition to this, biases in SST and heat flux components are discussed.

### 5 Sub-regional heat budget analysis

#### 5.1 Arabian Sea

Figure 6a illustrates the annual cycle of observed MLT tendency, net effect of mixed layer processes and the residual over the Arabian Sea. More prominently residual is much less than signals in most of the year. This residual in the observations arises due to errors in the different reanalysis products and numerical computations. The MLT tendency closely follows the HF cycle from fall to spring, suggesting the dominant role of HF in the annual cycle (Fig. 6b). Annual cycle of Hadv shows strong negative contribution

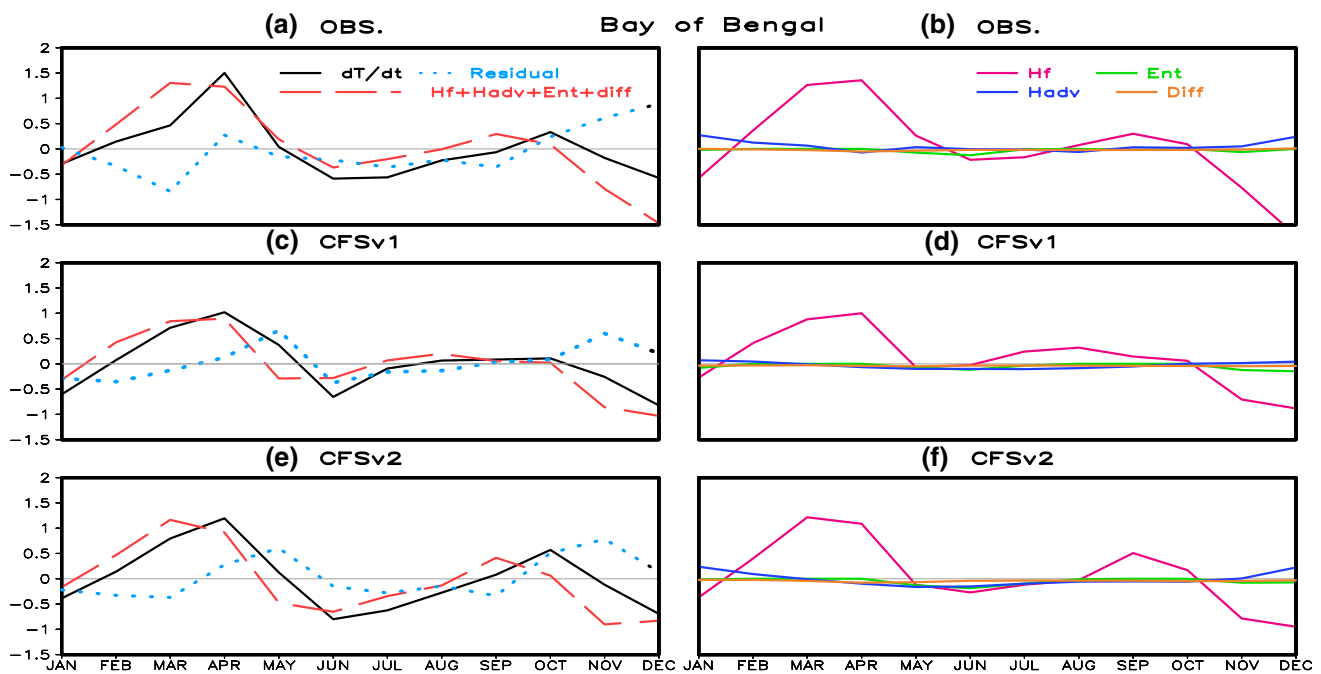


**Fig. 7** Same as in Fig. 6, but for the Bay of Bengal

during the summer months in the observations, which is consistent with the spatial distribution (Fig. 4j). Contribution of vertical entrainment and diffusion are weak throughout the year in the Arabian Sea compared to other processes. Temperature drop of about 2.5 °C from April to July and rise of about 2 °C from July to October is noted in the observations. This drop and rise in temperature tendency are very well explained by HF and Hadv.

CFSv1 displays a low rate of change of temperature over the Arabian Sea throughout the year, mainly during summer (Fig. 6c). This misrepresentation has been attributed to errors in HF and Hadv annual cycle (Fig. 6d). Heat budget equation may not completely close in the coupled models due to numerical errors and non-linear processes. The frequency of output used for heat budget also affects the budget closure. It is important to note that the residual is within the limits in most of the year. MLT tendency is well represented in CFSv2 than in CFSv1 (Fig. 6c, e). Rate of change of MLT is consistent with sum of all mixed layer processes except in June. Anomalous negative contribution of  $w_e$  is responsible for the higher residual (Fig. 6f). Compared to other processes contribution of Hadv is stronger in Arabian Sea cooling during summer in both the models and observations. CFSv1 and CFSv2 could capture the seasonal evolution of horizontal advection with the respective underestimation of 50 and 25 % during summer season. The weaker winds and the resultant ocean currents explain the underestimation of horizontal advection mainly during summer in CFSv1 (Fig. 6d). During winter, CFSv2 cold

MLT is explained by anomalous negative HF, which is consistent with previous coupled model studies (e.g., Turner et al. 2012; Marathayil et al. 2013).

## 5.2 Bay of Bengal

Bay of Bengal observed temperature tendency, sum of heat budget terms and the residual are displayed in Fig. 7a. Residual is slightly higher in the Bay of Bengal than Arabian Sea. This could be due to the complexity of mixed layer processes in this region. HF term appears to be the dominant contributor for changes in Bay of Bengal MLT (Fig. 7b). Contribution of other component of heat budget terms to MLT tendency is very weak. Temperature tendency in CFSv1 is represented poorly during the second half of the year (Fig. 7c). HF annual cycle shows strong coherency with MLT tendency, especially during summer where rate of change is low. This indicates that CFSv1 has problems in representing the annual cycle of heat flux components over the Bay of Bengal. The contributions from entrainment and horizontal advection are weaker compared to HF in this region for both the observations and models (Fig. 7b, d, f). CFSv2 displays better annual cycle of HF contribution to MLT tendency over the Bay of Bengal (Fig. 7e, f). For example, the gradual change of MLT from June to September is well represented in CFSv2 due to proper HF evolution. Such evolution in MLT and HF are wrongly represented in CFSv1. Over all MLT tendency over the Bay of Bengal is primarily determined by HF

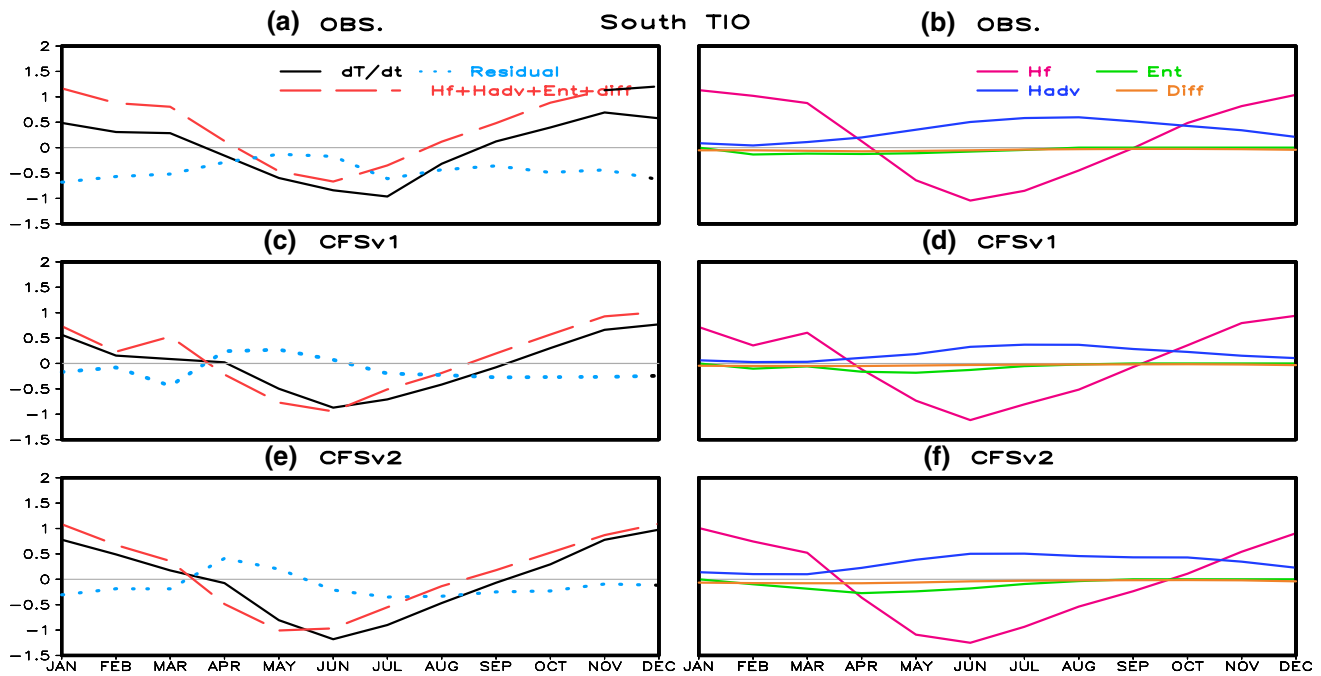


**Fig. 8** Same as in Fig. 6, but for the Southern Tropical Indian Ocean (STIO)

term. This suggests the importance of accuracy in the evolution of heat flux annual cycle in the coupled models.

### 5.3 Southern TIO

Over the STIO observations show strong cooling of MLT from May to August and warming in rest of the year (Fig. 8a). Residual is relatively less compared to signal. Strong cooling in summer is mainly contributed from HF term (Fig. 8b). On the other hand, Hadv is contributed positively to MLT change throughout the year with maximum contribution in late summer. Both HF and Hadv contributed positively to MLT tendency during winter and early spring. Contribution of other terms of Eq. 1 is weak. During summer season Hadv (positive contribution) is underestimated by about 50 % in CFSv1 and 10–20 % in CFSv2 over the STIO. The negative contribution of HF in CFSv2 during summer is slightly over estimated. This suggests that the problems in representing both these processes have contributed for the strong negative MLT tendency in CFSv2. Rate of change in MLT from winter to summer is relatively weak in CFSv1 compared to the observations (Fig. 8a, c, e). This low rate of change is mainly associated with weak HF annual cycle in CFSv1. Whereas in CFSv2, HF contributed for strong cooling in summer than in observations. Role of HF is supported further by spatial distribution (Fig. 4). Thus error in heat flux could modulate MLT tendency over the STIO region. Further contribution of Hadv is slightly weaker in CFSv1 as compared to CFSv2 and observations

(Fig. 8b, d, f). This could be mainly due to weak surface winds in CFSv1. Altogether, MLT tendency is dominated by HF and Hadv terms in both observations and models. Over-estimation of HF contribution in CFSv2 is associated with misrepresentation of heat flux components or heat flux bias.

### 5.4 South-eastern EIO and western EIO

Observation shows that MLT tendency over SEIO (eastern IOD box) is equally controlled by HF and Hadv terms (Fig. 9a, b). During summer magnitudes of HF and Hadv are largely balanced, which is clear in the observations and CFSv2. While the contribution of HF and Hadv is highly underestimated in CFSv1. In the rest of year both HF and Hadv contributes positively to MLT tendency in the observations. However, CFSv1 displays large changes in MLT from spring to summer over the SEIO unlike in observations (Fig. 9a, c). Annual cycle of Hadv and  $w_e$  is not well represented in CFSv1 (Fig. 9d) due to unrealistic surface winds. This is mainly responsible for the unrealistic cooling of MLT during August over this region. Large residual at the end of the calendar year is associated with poor representation of HF in CFSv1. Contribution of HF to MLT tendency is overestimated in CFSv2 over SEIO. Annual cycle of MLT tendency, HF and advective terms are better represented in CFSv2 compared to CFSv1 over SEIO.

MLT tendency in the observations over the western EIO (WEIO) shows two positive peaks one in April and other in October which is well represented in models (Fig. 10a,

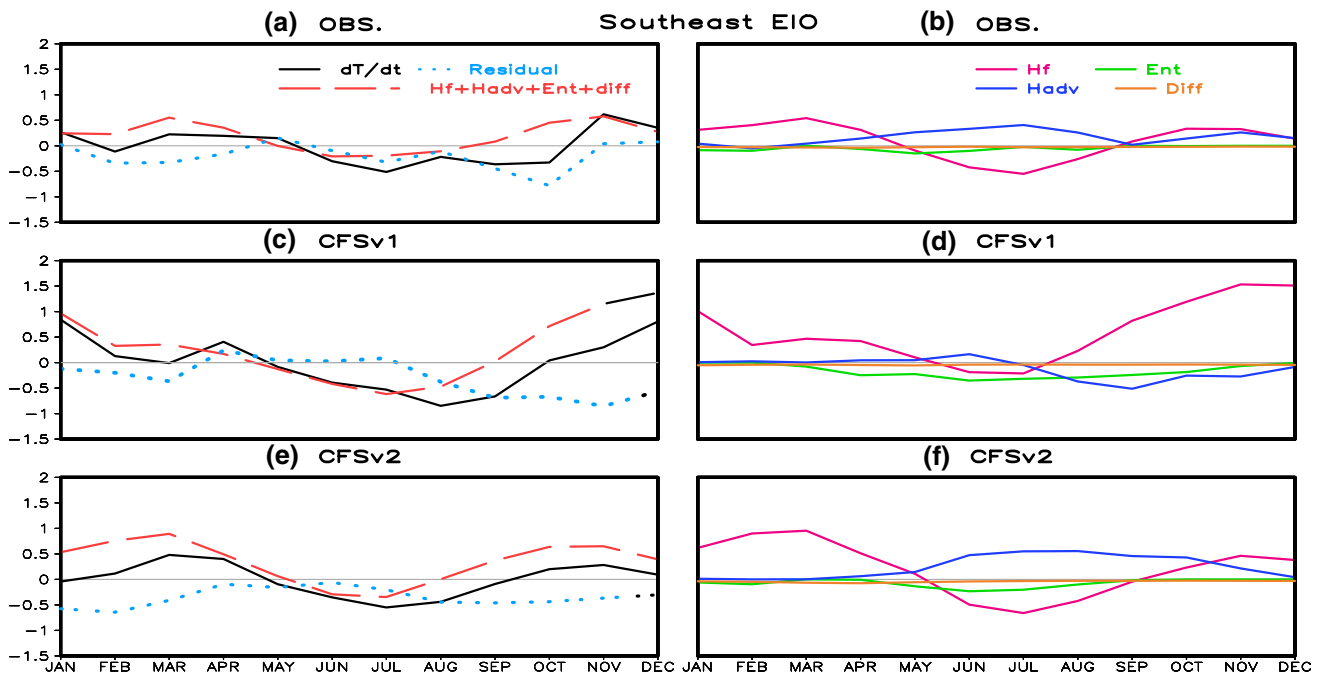


Fig. 9 Same as in Fig. 6, but for the southeastern equatorial Indian Ocean (SEIO)

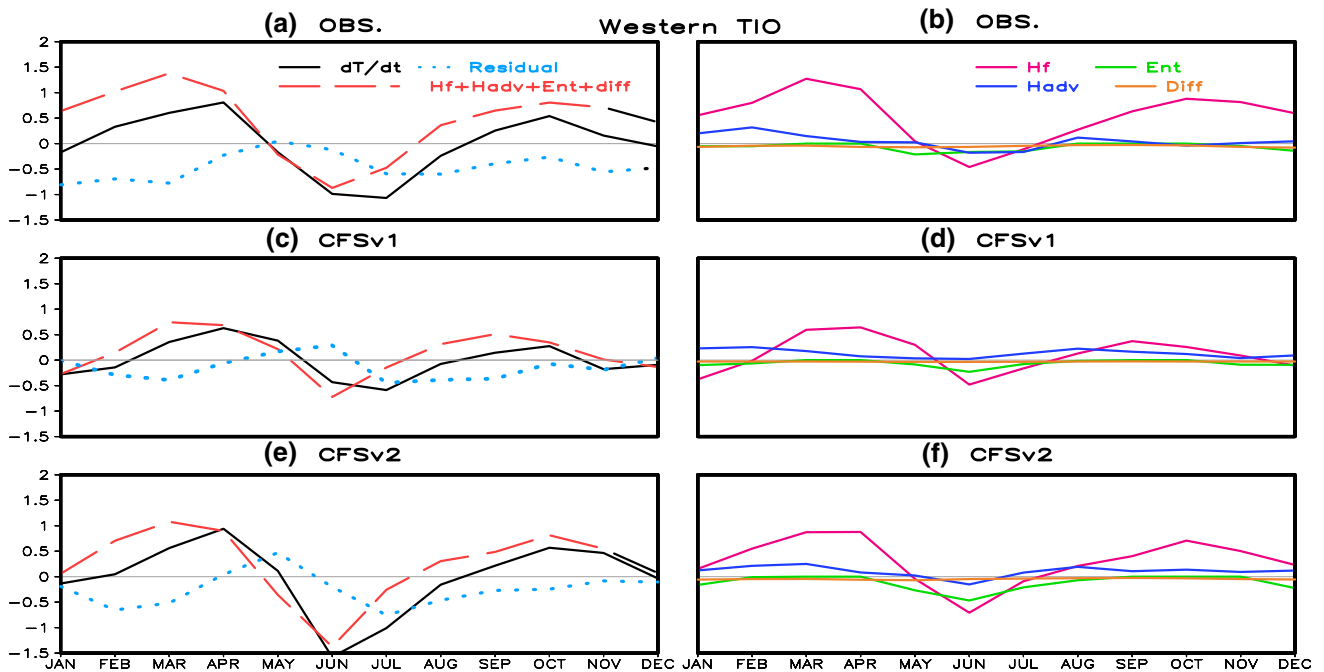
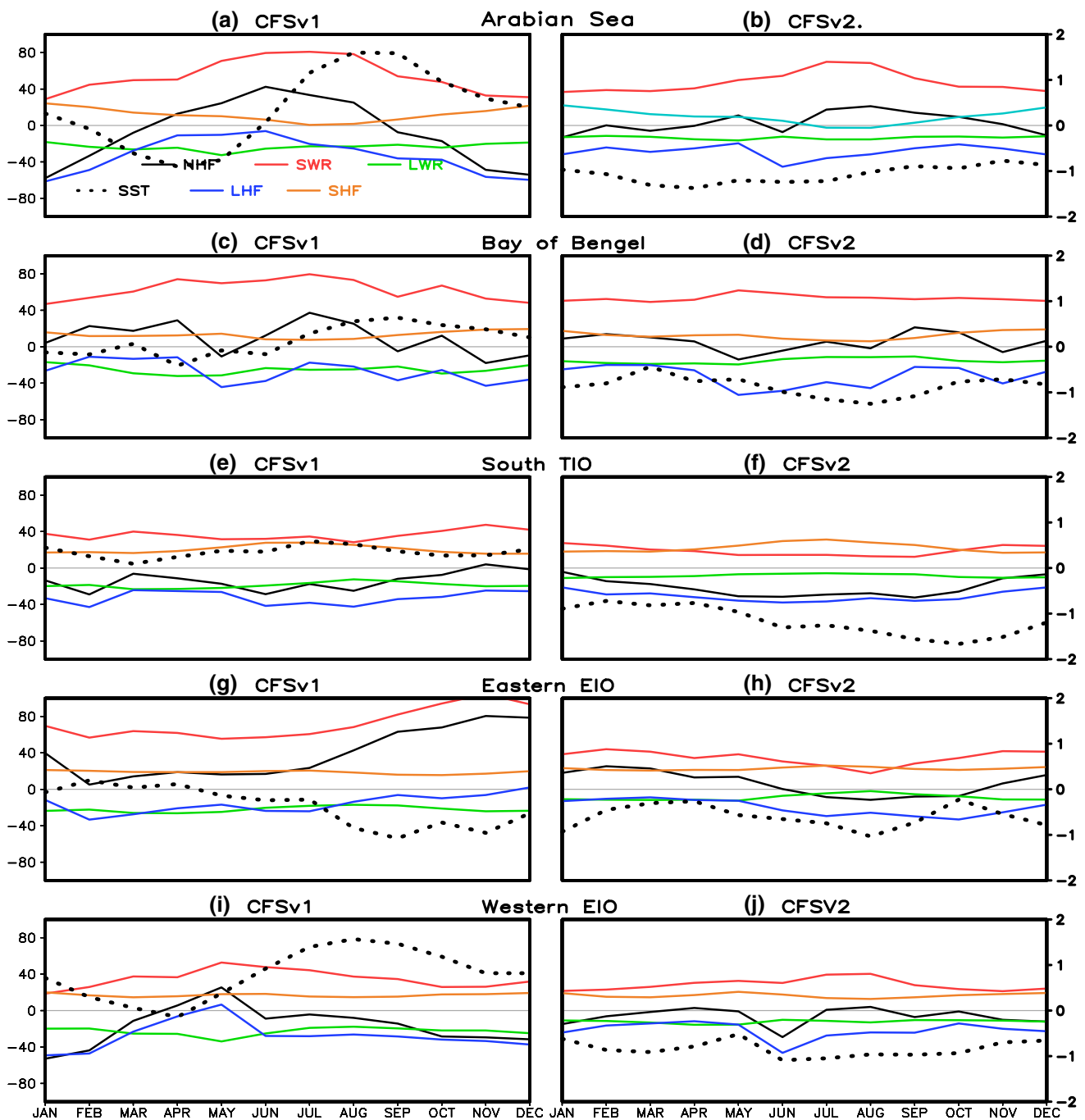


Fig. 10 Same as in Fig. 6, but for the western equatorial Indian Ocean (WEIO)

c, e). HF forcing mainly contributed for the changes in MLT over this region in the observations. Similar to Arabian Sea and STIO, rate of change of MLT is low in CFSv1 over WEIO (Fig. 10c). This low rate of change is associated with problems in HF representation (Fig. 10d). In case

of CFSv2, rate of change from spring to summer is high (Fig. 10e). Cooling during summer is contributed by  $w_e$  and HF term in CFSv2. Contribution of entrainment cooling to MLT during summer is stronger in CFSv2 compared to the observations. Thus it is important to represent the mixed



**Fig. 11** Biases in annual cycle of SST ( $^{\circ}\text{C}$ ), net heat flux ( $\text{W}/\text{m}^2$ ), shortwave radiation ( $\text{W}/\text{m}^2$ ), long wave radiation ( $\text{W}/\text{m}^2$ ), latent heat flux ( $\text{W}/\text{m}^2$ ) and sensible heat flux ( $\text{W}/\text{m}^2$ ) over different sub-regions of the TIO in CFSv1 (left) and CFSv2 (right)

layer processes well in coupled models in order to maintain proper MLT/SST cycle in different regions of TIO.

### 6 Bias in heat flux and SST annual cycle

Mixed layer heat budget analysis showed strong lead-lag relationship between net heat flux and MLT/SST evolution

(Figs. 6–10). This reveals that heat flux is critical in SST evolution over the TIO region. Thus errors/biases in heat flux may strongly influence the bias in SST annual cycle. Figure 11 illustrate bias (with respective to observations) in SST, net heat flux and heat flux components such as SWR, long wave radiation (LWR), latent heat flux (LHF) and sensible heat flux (SHF) in different regions of TIO for CFSv1 and CFSv2. Note that as the SST is tightly coupled with

the atmosphere in coupled models, bias in SST cannot be explained by heat flux alone. Thus here we discussed only the possible impact of heat flux bias on SST bias.

Lead–lag relationship between net heat flux and SST bias is evident over the Arabian Sea in CFSv1 (Fig. 11a). Net heat flux bias is positive during summer and as a response SST bias turned to positive. Strong bias ( $>50 \text{ W/m}^2$ ) in SWR during summer is responsible for positive net heat flux bias. During fall and winter, bias in LHF dominated the negative bias in heat flux over the Arabian Sea. CFSv1 shows that SST over the Bay of Bengal is cooler during the first half of the year as compared to the observations (Fig. 11c). This cold bias in the annual cycle is highly influenced by net heat flux bias which is contributed from errors in LWR and LHF. SST annual cycle is better represented by CFSv1 over the STIO, which is reflected in bias as well (Fig. 11e). Net heat flux bias is within  $25 \text{ W/m}^2$  in CFSv1 but with negative sign. Bias in LHF is balanced by SWR positive bias in CFSv1 over this region. In general bias in SWR is mainly responsible for the bias in the annual cycle of net heat flux in CFSv1. As in other regions, SWR and LHF have contributed to the changes in the annual cycle of SST over SEIO by modifying the net heat flux. Strong negative SST bias from summer to winter over the SEIO is due to Indian Ocean Dipole like spatial bias pattern and misrepresentation of ocean dynamics in CFSv1 (e.g., Chowdary et al. 2014). In contrast to SEIO, strong positive SST bias is noted over WEIO in CFSv1 from May to December (Fig. 10a). Net heat flux is negative from summer to winter suggesting that the bias in SST (warm bias) is not totally controlled by heat flux. It is important to note that SWR and LWR display systematic positive bias throughout the year (Fig. 11). Bias in SHF is smaller than other components of heat flux.

CFSv2 displays systematic cold bias throughout the year over Arabian Sea and Bay of Bengal (Fig. 11b, d). SWR and LWR (ocean loose) are overestimated over the Bay of Bengal throughout the year, with respective biases of about  $30\text{--}40$  and  $10\text{--}15 \text{ W/m}^2$ . LHF is also overestimated (negatively) by about  $30\text{--}40 \text{ W/m}^2$  and so underestimated the resultant net heat flux in the model as compared to the observations. These errors are mainly contributing towards the cool SST bias in CFSv2. Thus reducing errors in heat flux is essential for improving SST annual cycle or biases. SST bias is stronger especially in the second half of the year over STIO in CFSv2 (Fig. 11f). This bias/difference is clearly related to negative heat flux bias. Anomalous LHF with  $\sim 30 \text{ W/m}^2$  bias have strong influence on SST over the STIO. Net heat flux bias (negative) is about  $30 \text{ W/m}^2$  during June and July. Over all, the annual cycle of SST over the STIO is highly influenced by negative net heat flux bias in CFSv2. SST bias in SEIO and WEIO is negative throughout the year as in the other regions and to some

extent this bias is controlled by heat flux (Fig. 11h, j). Both CFSv1 and CFSv2 display systematic bias in SWR and LWR throughout the year in different regions.

Over all, CFSv2 produced better SST/MLT seasonal cycle though it has cold bias. This improvement in CFSv2 could be due to the up-gradation of different model physics. For example, improved physics for cloud–aerosol–radiation facilitates in reducing radiation biases. Updated land surface, ocean and sea ice processes, in addition to a new atmosphere–ocean–land data assimilation system and ocean component MOM4 improved the circulation and annual cycle of ocean–atmospheric components.

## 7 Summary

Predictability of monsoon precipitation in the coupled models comes from tropical SST (e.g., Wang et al. 2009). The potential role of the Indian Ocean SST variability in the Asian summer monsoon is explored by many previous studies (e.g., Clark et al. 2000; Yoo et al. 2006; Yang et al. 2007; Izumo et al. 2008; Xie et al. 2009; Levine et al. 2013). Thus accurate representation of tropical SST in coupled models is essential for monsoon prediction. However, a major limiting factor in capturing the rainfall in current coupled models comes from model deficiencies and misrepresentation of SST seasonal cycles over the Indian Ocean (e.g., Prodhomme et al. 2012). For example negative SST tendency over the Arabian Sea extended to April in CFSv1 unlike in observations and CFSv2 (Fig. 2), resulting delay in positive precipitation tendency in CFSv1 by a month over the ISM region. In CFSv2 strong rate of change in SST over the STIO is in coherent with strong negative precipitation tendency (Fig. 3j). Therefore the representation of SST seasonal cycle and its tendency over the TIO are very important for any dynamical operational forecasting system. Present study addresses the role of mixed layer processes in determining the SST seasonal cycle in the two coupled models CFSv1 and CFSv2. Spatiotemporal evolution of SST, surface winds and MLD are found to be better represented in CFSv2 than CFSv1 with respect to observations, though CFSv2 has cold SST bias with deeper MLD.

Low rate of change in Arabian Sea SST from spring to summer in CFSv1 ( $-0.5 \text{ }^\circ\text{C}$ ) compared to observations ( $-4 \text{ }^\circ\text{C}$ ) and CFSv2 ( $-3 \text{ }^\circ\text{C}$ ) is contributed by errors/bias in the net heat flux and horizontal advection. Over the EIO region drop in SST from spring to summer is higher (by about  $0.5 \text{ }^\circ\text{C}$ ) in CFSv2 than in the observations, which is also reflected in rainfall change over this region. CFSv1 displayed unrealistic upward vertical velocities during summer over the eastern EIO region and contributed for more than  $0.5 \text{ }^\circ\text{C}$  excess cooling as compared to the observations, leading to strong SST gradient in EIO. Further in



all seasons contribution of vertical velocity to SST change is misrepresented over the regions away from the equator in CFSv1. In CFSv2  $w_e$  contributed strongly to SST change in east of Sri Lanka in winter by 0.5 °C more than observations. Misrepresentation of entrainment velocity is well reflected in the spatial pattern of SST tendency/seasonal cycle in both the models. Contribution of heat flux to SST change is much stronger in CFSv2 compared to observations in the region south of 17°S in all seasons. Over STIO region contribution (magnitude) of horizontal advection term to SST change during fall in CFSv1 is underestimated by about 50 %. During winter strong horizontal advection is noted near Somalia coast in CFSv1 unlike in observation and CFSv2. The contribution of  $H_{adv}$  in winter is weak compared to that of summer and fall, and is evident both in observations and models. Thus large errors in heat flux and advective processes in models are responsible for the misrepresentation of seasonal changes in SST spatial pattern over most of the TIO. Seasonal tendency of SST in various regions of TIO is different from observations in both models. Seasonal evolution of SST and mixed layer processes are well represented in CFSv2 compared to CFSv1. This improvement may be due to the better representation of circulation and seasonal cycle of ocean–atmospheric components, which corresponds to improved physics for cloud–aerosol–radiation, updated land surface, ocean and sea ice processes, atmosphere–ocean–land data assimilation system and ocean component.

Sub-regional heat budget analysis reveals that CFSv1 is unable to reproduce the seasonal cycle of MLT tendency over the Arabian Sea, while CFSv2 captured the annual cycle of SST/MLT (bimodal distribution) with systematic cold bias. Rate of change in MLT is low throughout the year in CFSv1. The MLT tendency closely follows the net heat flux cycle, suggesting the dominant role of net heat flux in the annual cycle. Thus misrepresentation of HF annual cycle is accountable for low rate of change in MLT in most of the year. During summer  $H_{adv}$  also contributed for errors in MLT tendency in addition to HF in CFSv1. Horizontal advection during summer season is underestimated by 50 and 25 % respectively in CFSv1 and CFSv2. Heat budget analysis shows that residual is much less than the signals over most of the regions giving more meaning to the evaluation of the model MLT.

Residual is slightly higher in the Bay of Bengal than the Arabian Sea, which is due to the complexity of mixed layer processes in this region. HF term appears to be the dominant contributor for changes in Bay of Bengal MLT in both the observations and models. CFSv1 fails to represent proper HF annual cycle evolution and hence MLT tendency. Though CFSv2 HF annual cycle is well represented over the Bay of Bengal, its contribution to MLT change is underestimated compared to the observations. Over the

STIO, MLT tendency is dominated by HF and  $H_{adv}$  terms in both observations and models. Contribution of HF to MLT annual cycle tendency is overestimated (underestimated) in CFSv2 (CFSv1) especially during summer. While the contribution of  $H_{adv}$  to MLT change is underestimated by about 50 % in CFSv1 and 10–20 % in CFSv2. These errors in HF and  $H_{adv}$  are associated with biases in heat flux components and surface wind representation. Over the SEIO, CFSv1 has wrongly represented the contribution of HF,  $H_{adv}$  and  $w_e$  to MLT tendency mainly during the second half of the year. This is due to strong bias in the heat flux components and surface wind over this region. In case of CFSv2, contribution of HF is overestimated to MLT tendency annual cycle. HF forcing has mainly contributed for changes in MLT over WEIO in observations. Rate of change of MLT is low in CFSv1 over WEIO similar to Arabian Sea, which is due to problems in HF representation. In contrast the rate of change in MLT from spring to summer is high in CFSv2. This strong rate of change is associated with over estimation of  $w_e$  and HF term in CFSv2 during summer.

Altogether, mixed layer heat budget analysis reveals the existence of lead–lag relationship between net heat flux and MLT/SST evolution in observations and both the models. This suggests that heat flux is critical in SST evolution over the TIO region. Large biases in short wave and long wave radiation along with latent heat flux have been translated to net heat flux bias and have contributed to the SST annual cycle bias in CFSv1 and CFSv2. Though CFSv2 displays better skills in representing annual cycle of different ocean–atmospheric components, there exist strong bias especially in radiative and momentum flux components. This study advocates further improvements in the radiation parameterization and moisture processes in CFSv2 in order to obtain accurate seasonal SST changes over the TIO.

**Acknowledgments** We thank Director IITM for support. Sayantani acknowledge the support of Council of Scientific and Industrial Research (CSIR), India for Junior Research Fellowship. We sincerely thank anonymous reviewers for their valuable comments that helped us to improve the manuscript. We wish to thank H. S. Chaudhari, S. K. Saha and S. Pokhrel for providing model data. Figures are prepared using GrADS.

## References

- Annalai H (2010) Moist dynamical linkage between the equatorial Indian Ocean and the south Asian monsoon trough. *J Atmos Sci* 67:589–610
- Behera SK, Luo J-J, Masson S, Delecluse P, Gualdi S, Navarra A, Yamagata T (2005) Paramount impact of the Indian Ocean Dipole on the East African short rains: a CGCM study. *J Clim* 18:4514–4530
- Bollasina MA, Ming Y (2013) The general circulation model precipitation bias over the southwestern equatorial Indian Ocean and its

- implications for simulating the South Asian monsoon. *Clim Dyn* 40:823–838
- Boschat G, Terray P, Masson S (2012) Robustness of SST teleconnections and precursory patterns associated with the Indian summer monsoon. *Clim Dyn* 38:2143–2165
- Carton JA, Giese BS (2008) A reanalysis of ocean climate using Simple Ocean Data Assimilation (SODA). *Mon Weather Rev* 136:2999–3017
- Chaudhari HS, Pokhrel S, Saha SK, Ashish D, Yadav RK, Salunke K, Mahapatra S, Sabeerali CT, Rao SA (2013) Model biases in long coupled runs of NCEP CFS in the context of Indian Summer Monsoon. *Int J Climatol* 33:1057–1069. doi:10.1002/joc.3489
- Chowdary JS, Chaudhari HS, Gnanaseelan C, Parekh A, Rao SA, Sreenivas P, Pokhrel S, Singh P (2014) Summer monsoon circulation and precipitation over the tropical Indian Ocean during ENSO in the NCEP climate forecast system. *Clim Dyn* 42:1925–1947. doi:10.1007/s00382-013-1826-5
- Clark CO, Cole JE, Webster PJ (2000) Indian Ocean SST and Indian summer rainfall: predictive relationships and their decadal variability. *J Clim* 13:2503–2519
- Clough SA, Shephard MW, Mlawer EJ, Delamere JS, Iacono MJ, Cady-Pereira K, Boukabara S, Brown PD (2005) Atmospheric radiative transfer modeling: a summary of the AER codes. *J Quant Spectrosc Radiat Transf* 91:233–244
- de Boyer Montegut C, Mignot CJ, Lazar A, Cravatte S (2007) Control of salinity on the mixed layer depth in the world ocean: 1. General description. *J Geophys Res* 112:C06011. doi:10.1029/2006JC003953
- Du Y, Qu T, Meyers G, Masumoto Y, Sasaki H (2005) Seasonal heat budget in the mixed layer of the southeastern tropical Indian Ocean in a high-resolution ocean general circulation model. *J Geophys Res* 110:C04012. doi:10.1029/2004JC002845
- Ek MB, Mitchell KE, Lin Y, Rogers E, Grunmann P, Koren V, Gayno G, Tarplay JD (2003) Implementation of Noah land surface model advances in the National Centers for Environmental Prediction operational mesoscale Eta model. *J Geophys Res* 108(D22):8851. doi:10.1029/2002JD003296
- Griffies S, Harrison MJ, Pacanowski RC, Anthony R (2004) A technical guide to MOM4, GFDL ocean group technical report no. 5. NOAA/Geophysical Fluid Dynamics Laboratory, Princeton, 342 pp
- Hogg AM, Meredith MP, Blundell JR, Wilson C (2008) Eddy heat flux in the Southern Ocean: Response to variable wind forcing. *J Clim* 21:608–620
- Iacono MJ, Mlawer EJ, Clough SA, Morcrette J-J (2000) Impact of an improved longwave radiation model, RRTM, on the energy budget and thermodynamic properties of the NCAR community climate model, CCM3. *J Geophys Res* 105:14873–14890
- Izumo T, Montégut CD, Luo J-J, Behera SK, Masson S, Yamagata T (2008) The role of the western Arabian Sea upwelling in Indian monsoon rainfall variability. *J Clim* 21:5603
- Kara AB, Rochford PA, Hurlburt HE (2003) Mixed layer depth variability over the global ocean. *J Geophys Res.* doi:10.1029/2000JC000736
- Krishna Kumar K, Hoerling M, Rajagopalan B (2005) Advancing dynamical prediction of Indian Monsoon Rainfall. *Geophys Res Lett* 32:L08704. doi:10.1029/2004GL021979
- Lee JY, Wang B, Kang IS, Shukla J et al (2010) How are seasonal prediction skills related to models' performance on mean state and annual cycle? *Clim Dyn* 35:267–283
- Levine RC, Turner AG, Marathayil D, Martin GM (2013) The role of northern AS surface temperature biases in CMIP5 model simulations and future projections of Indian summer monsoon rainfall. *Clim Dyn* 41:155–172. doi:10.1007/s00382-012-1656-x
- Locarnini RA, Mishonov AV, Antonov JI, Boyer TP, Garcia HE, Baranova OK, Zweng MM, Johnson DR (2010) World Ocean Atlas 2009, volume 1: temperature. S. Levitus, Ed. NOAA Atlas NESDIS 68, U.S. Government Printing Office, Washington, DC, 184 pp
- Marathayil D, Turner AG, Shaffrey LC, Levine RC (2013) Systematic winter sea-surface temperature biases in the northern Arabian Sea in HiGEM and the CMIP3 models. *Environ Res Lett* 8:014028
- McCreary JP, Kundu PK, Molinari RL (1993) A numerical investigation of the dynamics, thermodynamics and mixed layer processes in the Indian Ocean. *Prog Oceanogr* 31:181–244
- Moorthi S, Pan HL, Caplan P (2001) Changes to the 2001 NCEP operational MRF/AVN global analysis/forecast system. *NWS Tech Proc Bull* 484:14
- Pacanowski RC, Griffies SM (1999) MOM 3.0 manual NOAA/Geophysical Fluid Dynamics Laboratory Rep, 680 pp
- Perigaud C, Delecluse P (1992) Annual sea-level variations in the tropical Indian Ocean from Geosat and shallow-water simulations. *J Geophys Res* 27:20169–20179
- Pokhrel S, Rahaman H, Parekh A, Saha SK, Dhakate A, Chaudhari HS, Gairola RM (2012) Evaporation–precipitation variability over Indian Ocean and its assessment in NCEP climate forecast system (CFSv2). *Clim Dyn* 39:2585–2608
- Praveen Kumar B, Vialard J, Lengaigne M, Murty VSN, McPhaden MJ (2010) TropFlux: air-sea fluxes for the global tropical oceans—description and evaluation against observations. *Clim Dyn* 38:1521–1543
- Prodhomme C, Masson S, Terray P, Izumo T, Tozuka T, Yamagata T (2012) Impacts of Indian Ocean SST biases on the Indo-Pacific climate as simulated in a global coupled model. *Geophysical Research Abstracts* 14, EGU2012-10020-1, EGU General Assembly 2012
- Prodhomme C, Terray P, Masson S, Izumo T, Tozuka T, Yamagata T (2014) Impacts of Indian Ocean SST biases on the Indian Monsoon: as simulated in a global coupled model. *Clim Dyn* 42:271–290. doi:10.1007/s00382-013-1671-6
- Qiu B (2000) Interannual variability of the Kuroshio extension system and its impact on the wintertime SST field. *J Phys Oceanogr* 30:1486–1502
- Qu T (2003) Mixed layer heat balance in the western North Pacific. *J Geophys Res* 108(C7):3242. doi:10.1029/2002JC001536
- Saha S, Nadiga S, Thiaw C, Wang J, Wang W, Zhang Q, van den Dool HM, Pan HL, Moorthi S, Behringer D, Stokes D, White G, Lord S, Ebisuzaki W, Peng P, Xie P (2006) The NCEP climate forecast system. *J Clim* 15:3483–3517
- Saha S, Moorthi S, Wu X, Wang J, Nadiga S, Tripp P, Pan HL, Behringer D, Hou Y-T, Chuang H-Y, Mark I, Michael E, Meng J, Yang R (2014) The NCEP climate forecast system version 2. *J Clim* 27:2185–2208. doi:10.1175/JCLI-D-12-00823.1
- Saha Subodh K, Pokhrel S, Chaudhari HS, Dhakate A, Shewale S, Sabeerali CT, Salunke K, Hazra A, Mahapatra S, Rao AS (2014) Improved simulation of Indian summer monsoon in latest NCEP climate forecast system free run. *Int J Climatol* 34:1628–1641. doi:10.1002/joc.3791
- Sahai AK, Sharmila S, Abhilash S, Chattopadhyay R, Borah N, Krishna RPM, Joseph S, Roxy M, De S, Pattnaik S, Pillai PA (2013) Simulation and extended range prediction of monsoon intraseasonal oscillations in NCEP CFS/GFS version 2 framework. *Curr Sci* 104(10):1394–1408
- Schott FA, Xie S-P, McCreary JP (2009) Indian Ocean circulation and climate variability. *Rev Geophys* 47:RG1002. doi:10.1029/2007RG000245
- Shankar D, Vinayachandran PN, Unnikrishnan AS, Shetye SR (2002) The monsoon currents in the north Indian Ocean. *Prog Oceanogr* 52:63–119
- Taschetto AS, Gupta AS, Hendon HH, Ummenhofer CC, England MH (2011) The relative contribution of Indian Ocean sea surface temperature anomalies on Australian summer rainfall during El Niño events. *J Clim* 24:3734–3747

- Turner AG, Joshi M, Robertson ES, Woolnough SJ (2012) The effect of Arabian Sea optical properties on SST biases and the South Asian summer monsoon in a coupled GCM. *Clim Dyn* 39(3–4):811–826. doi:[10.1007/s00382-011-1254-3](https://doi.org/10.1007/s00382-011-1254-3)
- Wang B, Kang I-S, Lee J-Y (2004) Ensemble simulations of Asian-Australian monsoon variability by 11 AGCMs. *J Clim* 17:803–818
- Wang B, Lee J-Y, Kang I-S, Shukla J, Kug J-S, Kumar A, Schemm J, Luo J-J, Yamagata T, Park C-K (2008) How accurately do coupled climate models predict the Asian-Australian monsoon inter-annual variability? *Clim Dyn* 30:605–619
- Wang B, Lee JY, Kang IS, Shukla J (2009) Advance and prospect of seasonal prediction: assessment of the APCC/CliPAS 14-model ensemble retrospective seasonal prediction (1980–2004). *Clim Dyn* 33:93–117. doi:[10.1007/s00382-008-0460-0](https://doi.org/10.1007/s00382-008-0460-0)
- Wu R, Kirtman BP (2007) Regimes of seasonal air–sea interaction and implications for performance of forced simulations. *Clim Dyn* 29:393–410. doi:[10.1007/s00382-007-0246-9](https://doi.org/10.1007/s00382-007-0246-9)
- Wu X, Moorthi KS, Okamoto K, Pan HL (2005) Sea ice impacts on GFS forecasts at high latitudes. Preprints, Eighth Conference on Polar Meteorology and Oceanography, San Diego, CA, Amer. Meteor. Soc., 7.4. <http://ams.confex.com/ams/pdfpapers/84292.pdf>
- Xie P, Arkin PA (1996) Analyses of global monthly precipitation using gauge observations, satellite estimates and numerical model predictions. *J Clim* 9:840–858
- Xie S-P, Hu K, Hafner J, Du Y, Huang G, Tokinaga H (2009) Indian Ocean capacitor effect on Indo-western Pacific climate during the summer following El Niño. *J Clim* 22:730–747
- Yang J, Liu Q, Xie S-P, Liu Z, Wu L (2007) Impact of the Indian Ocean SST basin mode on the Asian summer monsoon. *Geophys Res Lett* 34:L02708. doi:[10.1029/2006GL028571](https://doi.org/10.1029/2006GL028571)
- Yoo S-H, Yang S, Ho C-H (2006) Variability of the Indian Ocean sea surface temperature and its impacts on Asian-Australian monsoon climate. *J Geophys Res* 111:D03108. doi:[10.1029/2005JD006001](https://doi.org/10.1029/2005JD006001)
- Zheng Y, Shinoda T, Lin J-L, Kiladis GN (2011) Sea surface temperature biases under the stratus cloud deck in the Southeast Pacific Ocean in 19 IPCC AR4 coupled general circulation models. *J Clim* 24:4139–4164